European Commission

JRC TECHNICAL REPORTS

Least-square effective stiffness to be used with equivalent viscous damping as equivalent linear model

Molina Ruiz, F. J.

Pegon, P.

2017

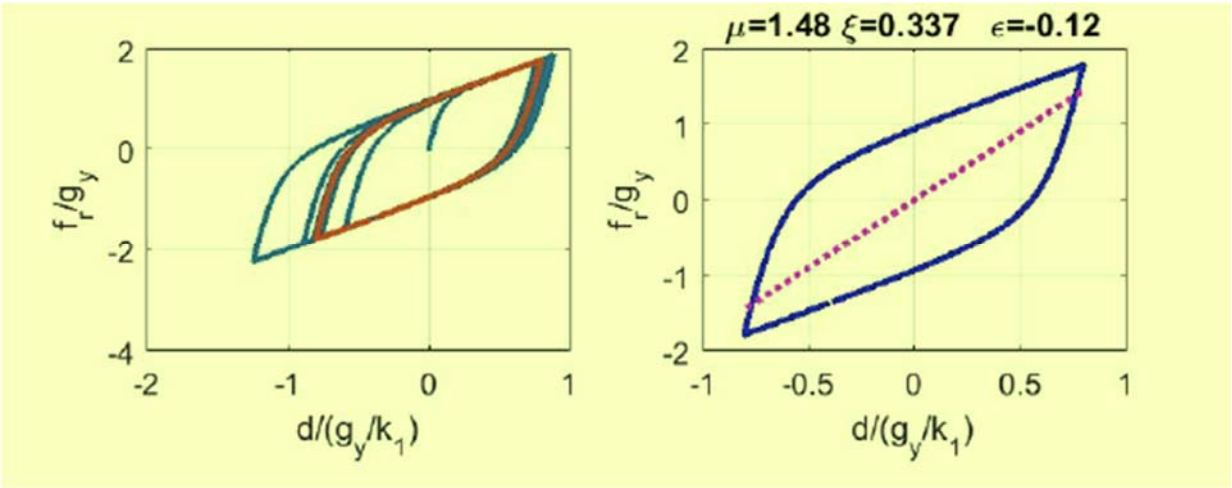

Joint Research Centre

EUR 28818 EN

JRC Science Hub
https://ec.europa.eu/jrc

JRC108427

EUR 28818 EN

PDF ISBN 978-92-79-74073-2 ISSN 1831-9424 doi:10.2760/40703

Luxembourg: Publications Office of the European Union, 2017

How to cite this report: Molina FJ and Pegon P, *Least-square effective stiffness to be used with equivalent viscous damping as equivalent linear model*, European Commission, EUR 28818 EN, doi:10.2760/40703

Contents

Foreword

This report is part of the deliverable "ELSALab report 2017" of "ELSALab - ELSA Laboratories" work package within the E4 Safety & Security of Buildings Unit, Directorate E - Space, Security and Migration of the JRC, European Commission.

Acknowledgements

The current work is performed within European Laboratory for Structural Assessment (ELSA) of the JRC E4 Safety & Security of Buildings Unit. Acknowledgement is given to all the colleagues and external collaborators contributing to the activites of the laboratory including this research.

Authors

Francisco Javier MOLINA RUIZ
Pierre PEGON

Abstract

This work introduces a method for the identification of linear stiffness and viscous damping parameters from a one-degree-of-freedom force-displacement cycle. Using an original approach, the stiffness parameter is derived by a least-square formula from the discrete input force-displacement point coordinates of the loop. The damping ratio is obtained in a classic manner from the quotient of absorbed and elastic energy. The obtained stiffness and damping parameters are proposed to be used, with the known mass, as an equivalent linear mass-spring-damper that should predict the response to a known load for the original nonlinear system associated to the input force-displacement cycle. As an example study, the effectiveness of such prediction is qualitatively shown for the case of the steady-state response to a harmonic load for a particular hysteretic numerical model by using a range of values for some dimensionless parameters. This kind of study is susceptible to be extended to other kinds of loading and numerical and experimental hysteretic models as well as to other identification procedures available in the literature.

1 INTRODUCTION

Proposals of equivalent linear mass-spring-damper models that may substitute a non-linear one-degree-of-freedom system are very difused in the literature and have gained relevance in the last decades especially with the development of displacement based design methods. Assuming that the mass is well known, two parameters (stiffness and viscous damping) need to be determined for the equivalent linear model. For systems with more degrees of freedom, also the choice of the mass represents another parameter, but such systems are out of the scope of current report.

As it is reported in the study produced by Dwairi et. al (2007) for example, the earliest contribution in this field is from Jacobsen (1930), who adopts as equivalent parameters a stiffness equal to the initial one and a damping coefficient based on the equality of the dissipated energy per cycle between the original nonlinear system and the substitute linear system. The same substitute system is adopted by the Direct Displacement-Based Design method for nonlinear structures proposed by Priestley (1993) with the difference of using the secant stiffness at the maximum reached displacement instead of the initial stiffness. The use of the secant stiffness combined with Jacobsen's equivalent damping was proposed by Rosenblueth and Herrera (1964) and is well perceived by the designers because of its simplicity in the computations and its natural integration with the use of linear design spectra. The passage from using the initial stiffness to the secant one and other proposed definitions of stiffness is also referred as period shift in the literature (e.g., Dwairi et. al, 2007).

In the current work, for the selection of the stiffness parameter, a different choice is done, which presumably represents an original approach. The stiffness is computed as the slope of the linear regression line of the force values with respect to the displacement values in the loop. This is equivalent to finding a straight line that minimizes the quadratic error of the force values with respect to it. Such slope will be called here least-square stiffness.

The concept of least-square identification is, of course, very difused and, in the experience of the authors, is also present in a different form in other equivalent linear models such as the Spatial Model, which, for example, are able to identify full matrices of stiffness and damping of multi-degree-of-freedom systems from the time response of the system in terms of force and displacement vectors (Ewins, 1984). We have proposed and extenselive used such model (Molina et al, 1999), particularly for the assessment of the errors in the seismic test setup system (Molina et al, 2011, 2013), but also for the prediction of the response of the structure itself to demand spectra different than the ones associated to the input data (Molina et al, 2016). At the same time, we have been also using the least-square stiffness for obtaining a linear approximation to experimental loops coming from cyclic tests and allowing to do predictions that were confirmed in many cases by the sucessive seismic experiments on the same specimen (Dal Lago and Molina, 2018, for example). The objective of the current work is to present the formulation of the least-square stiffness and the potential use of it.

In this report, the least-square stiffness identification, is combined with Jacobsen's equivalent damping, even though other possibilities can be imagined, and sucessively an example study is performed on the prediction error of such model for the steady-state response to harmonic loading. The numerical nonlinear law adopted for this demonstrative study is done by superposing a linear elastic force and a Giuffre and Pinto (1970) dissipative force.

2 PROPOSED METHOD FOR THE IDENTIFICATION

The method proposed here allows to identify a linear equivalent stiffness and a viscous equivalent damping from a given restoring force-displacement cycle. The relationship of the force-displacement data with time is ignored so that, in principle, they may come from any viscous or hysteretic model or any experimental measurements.

2.1 Energy ratio for a linear mass-spring-damper oscillator

The equivalence can be based on the assumption that the considered cycle is obtained during a period of oscillation at resonance of a single-degree-of-freedom linear viscous mass-spring-damper. Without knowing the time dependency, for that oscillator, the frequency itself and the mass cannot be identified, but the damping and the stiffness can be estimated from the shape of the cycle if we assume certain conditions to happen. The energy ratio is one of such conditions.

Consider first the motion of a linear mass-spring-damper oscillator:

$$ma + cv + kd = f_{ext}(t) \tag{1}$$

which is written under its canonical form as

$$a + 2\xi\omega v + \omega^2 d = \omega^2 f(t)/k \tag{2}$$

with the natural angular frequency ω and the viscous damping ratio ξ introduced as:

$$\omega^2 = \frac{k}{m} \qquad 2\xi\omega = \frac{c}{m} = \omega^2 \frac{c}{k} \tag{3}$$

When subjected to an external harmonic force

$$f_{ext}(t) = f_{ext}^0 \sin(\tilde{\omega}t) \tag{4}$$

in steady state, the system oscillates at the same angular frequency $\tilde{\omega}$ of the loading according to

$$\begin{aligned} d(t) &= D\sin(\tilde{\omega}t + \theta) \\ v(t) &= \tilde{\omega}D\cos(\tilde{\omega}t + \theta) \\ a(t) &= -\tilde{\omega}^2 D\sin(\tilde{\omega}t + \theta) \end{aligned} \tag{5}$$

with solution

$$D = \frac{f_{ext}^0/k}{\sqrt{(1-\tau^2)^2 + (2\xi\tau)^2}} \qquad \theta = tan^{-1}\left(\frac{2\xi\tau}{\tau^2 - 1}\right) \qquad \tau = \frac{\tilde{\omega}}{\omega} \tag{6}$$

The maximum amplitude of this oscillation (resonance) is obtained for a frequency close to the natural frequency

$$\frac{\tilde{\omega}_{RESONANCE}}{\omega} = \tau_{RESONANCE} = \sqrt{1 - 2\xi^2} \tag{7}$$

for which the maximum amplitude of displacement D is reached as

$$D_{RESONANCE} = \frac{f_{ext}^0/k}{2\xi\sqrt{1-\xi^2}} \tag{8}$$

Consider now the total structural (restoring) force

$$f_r = cv + kd \tag{9}$$

As a function of d. An example is shown in **Figure 1** for $k = 1,\ \omega = 1,\ \delta = 1$ and $\xi = 15/100$.

Figure 1 – Force & displacement vs. time (left) and force vs. displacement (right)

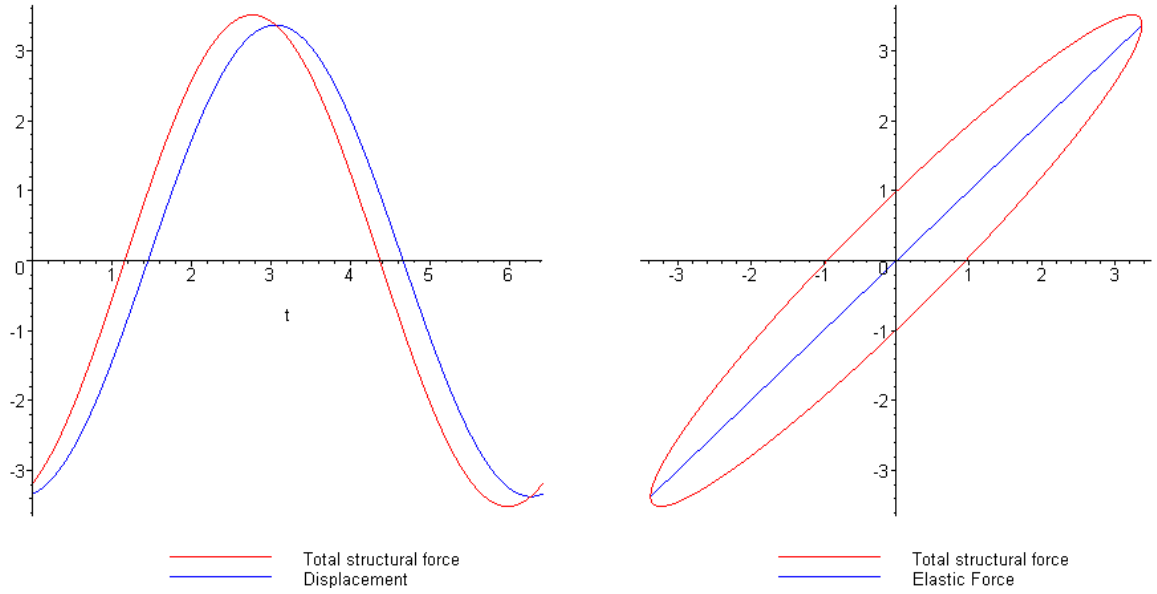

The integral of this force over the displacement cycle gives the dissipated energy

$$E_{abs} = \oint f_r(d)\mathrm{d}d = \int_0^{2\pi/\tilde{\omega}} f_r(t)\, v\ \mathrm{d}t = \int_0^{2\pi/\tilde{\omega}} (cv + kd)\, v\ \mathrm{d}t \tag{10}$$

And, according to equation (5), clearly the same results are obtained considering only the viscous force in the integral.

$$E_{abs} = \int_0^{2\pi/\tilde{\omega}} cv^2\ \mathrm{d}t = \frac{1}{2}\frac{2\pi}{\tilde{\omega}} c\mathrm{D}^2\tilde{\omega}^2 = \pi c\mathrm{D}^2\tilde{\omega} \tag{11}$$

Then, the maximum elastic energy stored during the cycle is obtained for $d = D$ as

$$E_{el} = \frac{k\mathrm{D}^2}{2} \tag{12}$$

giving an energy ratio of

$$\frac{E_{abs}}{E_{el}} = \frac{2\pi c\tilde{\omega}}{k} = \frac{4\pi\xi\tilde{\omega}}{\omega} \tag{13}$$

which, when exciting at the natural frequency, leads exactly to

$$\frac{E_{abs}}{4\pi E_{el}} = \xi \tag{14}$$

and, at the frequency of resonance (7), anyway leads to approximately the same value

$$\frac{E_{abs}}{4\pi E_{el}} = \xi\sqrt{1-2\xi^2} = \xi + \xi^3 + O(\xi^5) \approx \xi \tag{15}$$

Formula (14) was proposed by Jacobsen (1930). Note that for applying formula (14), the shape of the loop is used for obtaining the absorbed energy, but an additional condition allowing the estimation of the stiffness is also required for obtaining the elastic energy. In the following section, least-square identification for the estimation of the stiffness is presented.

It must be noted that, in the case of a force-displacement loop coming from a viscous model, the determination of the damping ratio based on the energy quotient (14) may be far from accurate for predictions of the response to harmonic load if the excitation frequency is not confirmed to be close to the natural one (see equation (13)). On the other hand, the most interesting application of such formula should be for loops coming from hysteretic models as it is typical in the literature (a short example study on the prediction error for such a case is included in the current document at Chapter 3).

2.2 Estimation of the stiffness by a least-square (LS) approach

While the estimation of the damping ratio based on the quotient of energy (14) is used by many authors, for the estimation of the stiffness, we propose here an approach, based on a least square identification, that we consider original.

Let us define an approximation of the restoring force as a linear function of the displacement

$$\overline{f_r}(t) = f_0 + k_{LS}\, d(t) \tag{16}$$

where f_0 is the zero ordinate and k_{LS} is the slope of the line. The square "error" or ordinate distance of the restoring force data $f_r(t)$ to the straight line $\overline{f_r}$ (16) is

$$\varepsilon(f_0, k_{LS}) = \int_0^T (f_r(t) - \overline{f_r}(t))^2 \mathrm{d}t \tag{17}$$

which minimization with respect to the f_0 and k_{LS} parameters yields to the equations

$$\begin{aligned} \int_0^T f_r(t)\mathrm{d}t &= f_0 \int_0^T \mathrm{d}t + k_{LS}\int_0^T d(t)\mathrm{d}t \\ \int_0^T f_r(t)d(t)\mathrm{d}t &= f_0 \int_0^T d(t)\mathrm{d}t + k_{LS}\int_0^T d^2(t)\mathrm{d}t \end{aligned} \tag{18}$$

The solution of equations (18) renders the LS (least-square) identified stiffness

$$k_{LS} = \frac{T\int_0^T f_r(t)d(t)\mathrm{d}t - \int_0^T f_r(t)\mathrm{d}t \int_0^T d(t)\mathrm{d}t}{T\int_0^T d^2(t)\mathrm{d}t - \left(\int_0^T d(t)\mathrm{d}t\right)^2} \tag{19}$$

and the zero ordinate of the linear model

$$f_0 = \frac{\int_0^T f_r(t)\mathrm{d}t - k_{LS}\int_0^T d(t)\mathrm{d}t}{T} \tag{20}$$

being

$$T = \int_0^T \mathrm{d}t \tag{21}$$

the time duration of the cycle. In fact, equations (19) and (20) represent the linear regression of the force-displacement loop.

Two interesting properties of the LS stiffness estimation (19) for two types of generic problems will be pointed out now in the following two subsections.

2.2.1 LS stiffness in the case of a linear spring with a viscous damper

In the case of a linear spring with a viscous damper represented by equation (9), from the definition (19) we have that

$$\begin{aligned} k_{LS} &= \frac{T\int_0^T (cv(t)+kd(t))d(t)\mathrm{d}t - \int_0^T (cv(t)+kd(t))\mathrm{d}t\int_0^T d(t)\mathrm{d}t}{T\int_0^T d^2(t)\mathrm{d}t - \left(\int_0^T d(t)\mathrm{d}t\right)^2} \\ &= \frac{T\left(c\int_0^T v(t)d(t)\mathrm{d}t + k\int_0^T d^2(t)\mathrm{d}t\right) - \left(c\int_0^T v(t)\mathrm{d}t + k\int_0^T d(t)\mathrm{d}t\right)\int_0^T d(t)\mathrm{d}t}{T\int_0^T d^2(t)\mathrm{d}t - \left(\int_0^T d(t)\mathrm{d}t\right)^2} \end{aligned} \tag{22}$$

Then, assuming a closed displacement loop,

$$\int_0^T v(t)d(t)\mathrm{d}t = \int_{d(0)}^{d(T)} d\,\mathrm{d}d = \frac{d^2(T)-d^2(0)}{2} = 0 \tag{23}$$

and

$$\int_0^T v(t)\mathrm{d}t = \int_{d(0)}^{d(T)} \mathrm{d}d = d(T) - d(0) = 0 \tag{24}$$

Which results in the property of the LS stiffness of being equal to the stiffness of the original spring independently of the time variation of the displacement as far as it represents a closed loop

$$k_{LS} = k \tag{25}$$

2.2.2 LS stiffness in the case of a general nonlinear loop of fixed shape

On the other hand, for a general nonlinear hysteretic loop of fixed shape, even though the LS stiffness defined by equation (19) may depend on the particular time variation of the displacement and force, its value is not altered when the time variable is multiplied by any constant scale factor λ. Say

$$t = \lambda t_1; \quad T = \lambda T_1 \tag{26}$$

with a constant loop shape that does not depend on the time scale

$$d(t) = d_1(t_1); \quad f_r(t) = f_{r1}(t_1) \tag{27}$$

Then

$$\begin{aligned}[k_{LS}]_t &= \frac{T\int_0^T f_r(t)d(t)\mathrm{d}t - \int_0^T f_r(t)\mathrm{d}t \int_0^T d(t)\mathrm{d}t}{T\int_0^T d^2(t)\mathrm{d}t - \left(\int_0^T d(t)\mathrm{d}t\right)^2} \\ &= \frac{\lambda T_1 \int_0^{T_1} f_{r1}(t_1)d_1(t_1)\lambda\mathrm{d}t_1 - \int_0^{T_1} f_{r1}(t_1)\lambda\mathrm{d}t_1 \int_0^{T_1} d_1(t_1)\lambda\mathrm{d}t_1}{\lambda T_1 \int_0^{T_1} {d_1}^2(t_1)\lambda\mathrm{d}t_1 - \left(\int_0^{T_1} d_1(t_1)\lambda\mathrm{d}t_1\right)^2} \\ &= \frac{T_1 \int_0^{T_1} f_{r1}(t_1)d_1(t_1)\mathrm{d}t_1 - \int_0^{T_1} f_{r1}(t_1)\mathrm{d}t_1 \int_0^{T_1} d_1(t_1)\mathrm{d}t_1}{T_1 \int_0^{T_1} {d_1}^2(t_1)\mathrm{d}t_1 - \left(\int_0^{T_1} d_1(t_1)\mathrm{d}t_1\right)^2} = [k_{LS}]_{t_1}\end{aligned} \tag{28}$$

Showing that, assuming a pure hysteretic behaviour, the result does not depend on the adopted time scale, or frequency of oscillation.

2.3 Proposed procedure for the identification method

For practical application, the procedure for the estimation of the equivalent linear stiffness and damping starts from the given discrete values of restoring force and displacement of the cycle.

Namely, if the data of the force-displacement loop is given as discrete points

$$f_r(n) = f_r(t_n); \quad d(n) = d(t_n) \qquad n = 1 \dots N \tag{29}$$

The minimization of the square "error" of the force values with respect to a straight line

$$\overline{f_r}(n) = f_0 + k\, d(n) \tag{30}$$

Leads to the LS estimated stiffness given by the linear-regression formula

$$k_{LS} = \frac{N\sum(d(n)\, f_r(n)) - (\sum d(n))\sum f_r(n)}{N\sum d(n)^2 - (\sum d(n))^2} \tag{31}$$

which is the discrete version of equation (19).

Now, the absorbed energy is computed using the trapezoidal rule as

$$\hat{E}_{abs} = \sum_{n=2}^{N} f_{av}(n)(d(n) - d(n-1)) \tag{32}$$

where $f_{av}(n)$ is the average force

$$f_{av}(n) = \frac{f_r(n) + f_r(n-1)}{2} \tag{33}$$

Then, for the estimation of the elastic energy, the loop amplitude is computed as

$$\mathrm{D} = \frac{d_{max} - d_{min}}{2} \tag{34}$$

and

$$\hat{E}_{el} = k_{LS}\mathrm{D}^2/2 \tag{35}$$

Finally, the damping ratio estimation is derived from expression (14) as

$$\hat{\xi} = \frac{\hat{E}_{abs}}{4\pi\hat{E}_{el}} \tag{36}$$

3 EXAMPLE OF PREDICTION ERROR STUDY FOR THE PROPOSED EQUIVALENT STIFFNESS AND DAMPING

In this study, the performance of the proposed method for the identification of equivalent stiffness and damping will be partially assessed. It does not pretend to be a complete study, but rather a working example since it covers only the case of steady-state response to harmonic load for a particular analytical model of restoring force.

3.1 Analytical hysteretic model for the input force-displacement cycle

The model used for the current study comprises two terms. That is to say, the restoring force

$$f_r(d) = f_{el}(d) + g(d) \tag{37}$$

is modelled as the addition of an elastic force f_{el} and a dissipative hysteretic force g.

The elastic force is modelled by a power law on the displacement

$$f_{el}(d) = sign(d) k_1 D_1 \left|\frac{d}{D_1}\right|^q = k_1 d \left|\frac{d}{D_1}\right|^{q-1} \tag{38}$$

where q is a constant exponent, D_1 is a reference displacement point and k_1 is the secant stiffness at D_1 (see **Figure 2**, where the continuous line represents f_{el} and the dashed lines represents k_1).

Figure 2 – Example of elastic force term defined through a power function of the displacement ($q = 2$).

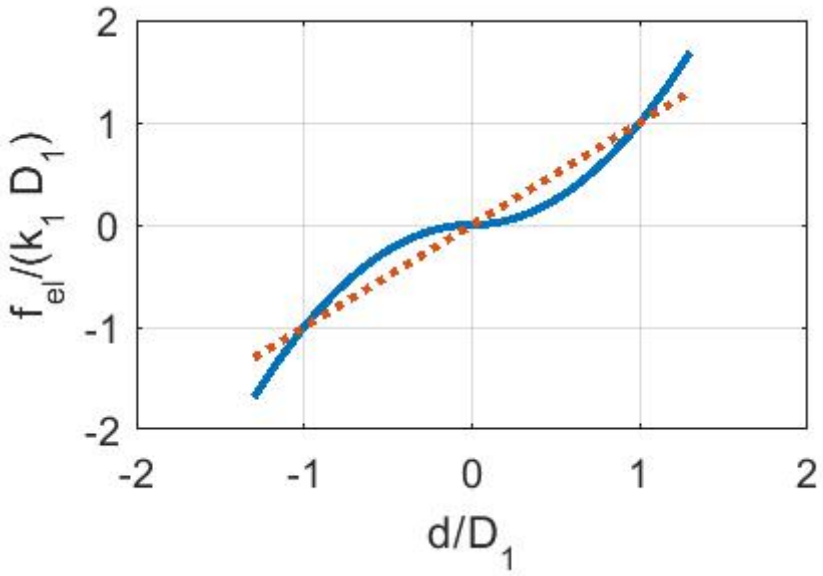

The dissipative force is modelled as purely hysteretic by a Giuffre and Pinto (1970) law

$$g^* = \frac{d^*}{(1 + |d^*|^R)^{1/R}} \tag{39}$$

where the normalized force is defined as

$$g^* = \frac{g - g_{RETURN}}{g_{CORNER} - g_{RETURN}} \tag{40}$$

and the normalized displacement as

$$d^* = \frac{d - d_{RETURN}}{d_{CORNER} - d_{RETURN}} \tag{41}$$

as represented in **Figure 3**. The asymptote (39) allows to pass smoothly from the initial stiffness k_{DAMP}, to the yield strength g_y. For the first loading branch, the return point $P_{RETURN}(d_{RETURN}, g_{RETURN})$ is taken as the origin of the axis. For successive unloading and reloading curves, the return point is the last point of the previous asymptotic path. The corner point of every loading phase $P_{CORNER}(d_{CORNER}, g_{CORNER})$ is the corner of the asymptote or intersection of its initial stiffness line with the yielding force $+g_y$ or $-g_y$. For example, for the first loading branch, the corner point is $(g_y/k_{DAMP}, g_y)$.

Figure 3 – Dissipative force term defined through a Giuffre and Pinto (1970) model.

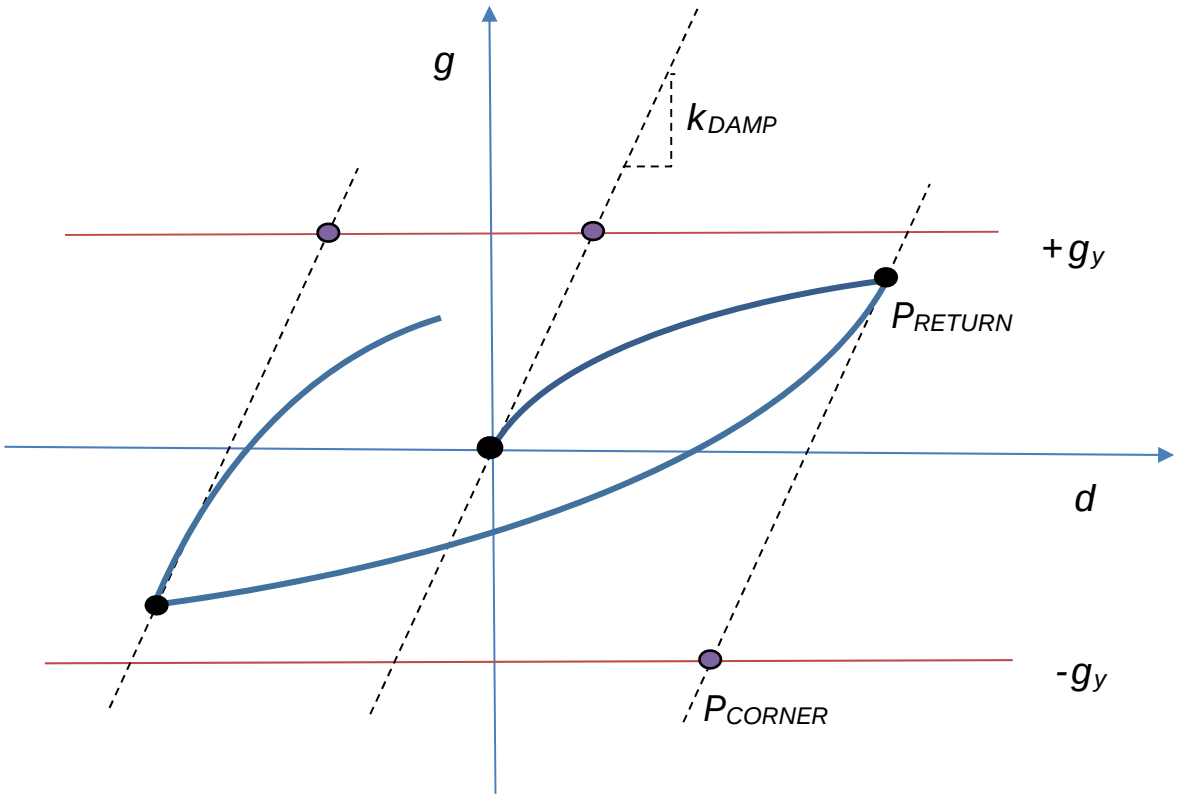

In the case of the exponent q being equal to 1, i.e.,

$$q = 1 \tag{42}$$

the elastic force (38) reduces to the linear case

$$f_{el}(d) = k_1 d \tag{43}$$

and, with the addition of the adopted dissipative law, the resulting restoring force model becomes equivalent to the Menegotto and Pinto (1972) model that allows for linear stress hardening. For values of q larger than 1 or smaller, the model of restoring force defined here allows for representing a wide range of interesting cases with, respectively, increasing (**Figure 4**a) or decreasing (**Figure 4**b) secant stiffness. Nevertheless, as a first approach for the current study, only the linear elastic force case (42),(43) will be considered (**Figure 4**c).

Figure 4 – Adopted restoring force model. Examples for different values of q.

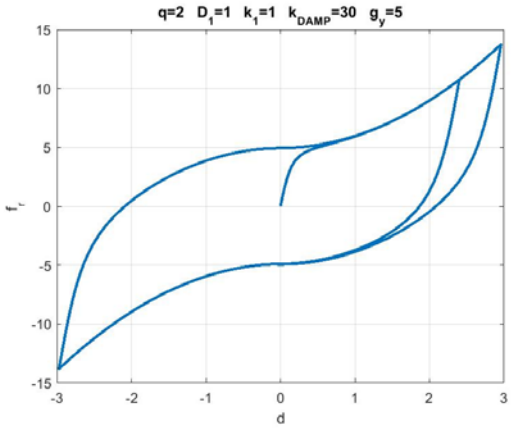

(a) $q > 1$

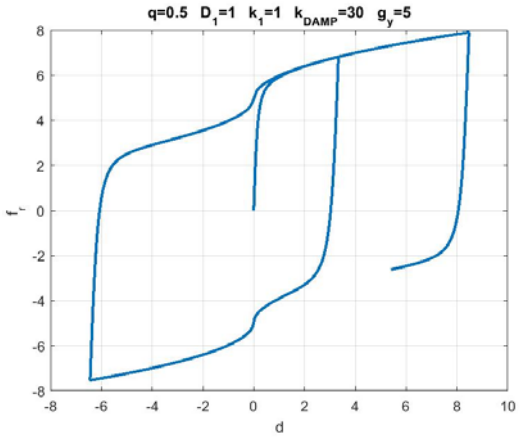

(b) $q < 1$

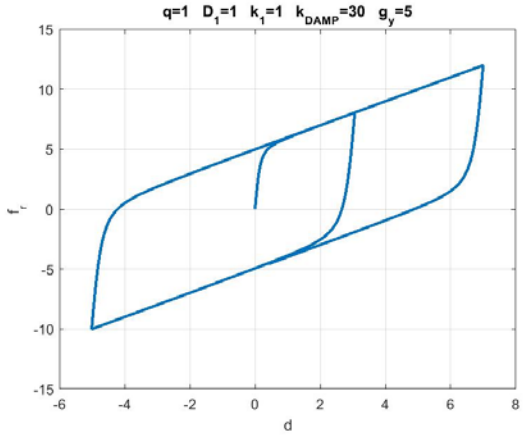

(c) $q = 1$

3.2 Computation of the steady-state response for a harmonic excitation

This study is limited to the analysis of force-displacement loops that are obtained as the steady-state response of the adopted restoring force model to a harmonic input load. Thus, instead of the linear equation (1), in this case, the equation of motion is the non linear one

$$ma + f_r(d) = f_{ext}(t) \tag{44}$$

where the restoring force f_r is computed through the model (37) described in the previous section, and the external harmonic load is given by equation (4).

In order to obtain the steady-state response, equation (44) is solved by using explicit Newmark (1959) method (by taking $\beta = 0$ and $\gamma = 1/2$), which is equivalent to the central difference method. In order to guarantee a high accuracy in the results, the time increment for the integration Δt is obtained by dividing the excitation period

$$\tilde{T} = \frac{2\pi}{\tilde{\omega}} \tag{45}$$

by an integer number which is chosen to be

$$N_{pcyc} = N_{pcyc0} \cdot MAX\{1, int\left(\frac{\tilde{T}}{2\pi\sqrt{m/(k_{DAMP} + k_1)}}\right)\} \tag{46}$$

i.e.,

$$\Delta t = \tilde{T}/N_{pcyc} \tag{47}$$

This means that the excitation period is divided in N_{pcyc0} increments at least, depending on the comparison of it with a rough estimation of the minimum natural period for the non-linear system

$$2\pi\sqrt{m/(k_{DAMP} + k_1)} \leq T_{natural} \tag{48}$$

For the results that will be presented in the current work, the basic (minimum) number of steps has been taken

$$N_{pcyc0} = 300 \tag{49}$$

However, all the computations have been repeated for a larger number of steps ($N_{pcyc0} = 500$), without significant change in the results for most of the cases, allowing to confirm that the convergence was achieved. The cases that we have found of no convergence are commented in the next section.

For the selected values of the model and excitation parameters, the integration is performed starting with zero value of displacement, velocity and restoring force.

In order to distinguish when the steady state has been reached, at the end of every time interval of duration $\tilde{T}$ (or N_{pcyc} time increments), the displacement amplitude for that excitation period is computed as half of the pick-to-pick displacement within that interval

$$D_{icyc} \leq \left(max(d)_{icyc} - min(d)_{icyc}\right)/2 \tag{50}$$

Then, the steady state is considered to be achieved when, between two consecutive cycles, that amplitude does not differ more than a tolerance of, say, 10^{-5} in relative terms, i.e.,

$$\left|D_{icyc} - D_{icyc-1}\right|/D_{icyc-1} \leq 10^{-5} \tag{51}$$

If the steady state is achieved within a limited number excitation periods (say 50), the integration is considered to be finished with a successful result, which is the obtained restoring force-displacement loop during the last excitation period $icyc$, that is to say,

$$[\ f_r(n) = f_r(t_n);\quad d(n) = d(t_n)\ ]_{\ n=\left((icyc-1)N_{pcyc}+1\right)\ldots\ icyc\cdot N_{pcyc}} \tag{52}$$

In **Figure 5**, an example of the integrated transient response (blue lines) with the converged steady-state cycle (red lines) is shown.

Figure 5 – Example of transient response that converges to steady state.

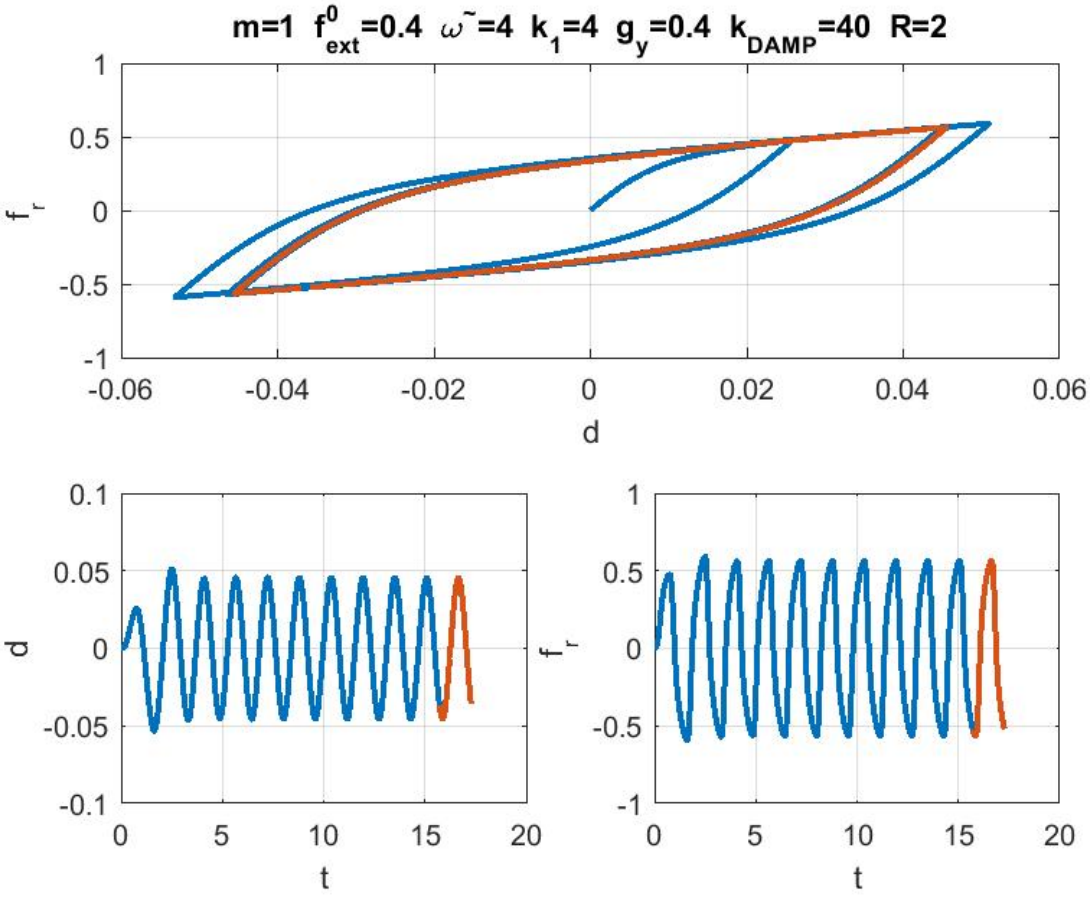

3.3 Parametric study of the prediction error

The proposed hysteretic restoring force model (37) and integration method for the numerical generation of the steady-state response of the equation of motion (44) to the harmonic excitation (4) are used for this parametric study. Then the obtained steady-state force-displacement loop (52) (red line in the example of **Figure 5**) is used as input for the determination of the estimated least-square stiffness (31) and the equivalent damping ratio (36). The performance of the estimated stiffness and equivalent damping parameters is afterwards assessed by defining a prediction error of the steady-state displacement amplitude as

$$\varepsilon = (D_{PRED} - D)/D \tag{53}$$

where, as in expression (50), the amplitude D is defined as half of the peak-to-peak displacement within the input interval (52) and, similarly to equation (6), the predicted amplitude by the proposed estimated stiffness and damping is

$$D_{PRED} = \frac{f_{ext}^0/k_{LS}}{\sqrt{(1-\mu^2)^2 + \left(2\hat{\xi}\mu\right)^2}} \qquad \mu = \frac{\tilde{\omega}}{\sqrt{k_{LS}/m}} \tag{54}$$

Before presenting results of the error for several ranges of values for some of the parameters of the model, we will transform it from its original variables listed in the implicit equation

$$h\left(m, f_{ext}^{0}, \widetilde{\omega}, k_1, D_1, g_y, k_{DAMP}, R, q, \varepsilon\right) = 0 \tag{55}$$

to the dimensionless ones used in

$$H(\Omega, \Phi, \Lambda, R, q, \Gamma, \varepsilon) = 0 \tag{56}$$

and defined as it follows

$$\Omega = \widetilde{\omega}/\sqrt{k_1/m} \tag{57}$$

$$\Phi = f_{ext}^{0}/g_y \tag{58}$$

$$\Lambda = k_{DAMP}/k_1 \tag{59}$$

$$\Gamma = D_1 k_1/g_y \tag{60}$$

with R already introduced by equation (39) and q by equation (38) that were originally defined as dimensionless constants and with ε defined at equation (53) being also dimensionless.

Note that the time instant variable has not been included in equation (55) since the error (53) is based only on the steady-state loop shape. The basic magnitudes involved in the 10 variables contained in equation (55) are 3 (mass, time and space), which, according to Buckingham π theorem, allows to work instead with 7 independent dimensionless variables as it is done in equation (56).

Then, by limiting the current study to the case of forcing the elastic component of the restoring force to be linear, i.e., following equations (42),(43), the parameters q and D_1 are removed from the model in its dimensional version

$$\bar{h}\left(m, f_{ext}^{0}, \widetilde{\omega}, k_1, g_y, k_{DAMP}, R, \varepsilon\right) = 0 \tag{61}$$

and q and Γ are also removed for the dimensionless one

$$\bar{H}(\Omega, \Phi, \Lambda, R, \varepsilon) = 0 \tag{62}$$

Note that in this case the basic magnitudes involved in the 8 variables contained in equation (61) are still 3, which allows to work instead with 5 independent dimensionless variables in equation (62).

Now, by taking as independent parameters the first four ones included in the formulation (62), the following discrete values, with all their combinations, have been used for the computation of the error:

$$\Omega = 0.1, 0.2, \ldots, 3.0 \tag{63}$$

$$\Phi = 0.05, 0.10, \ldots, 4.95 \tag{64}$$

$$\Lambda = 10, 100 \tag{65}$$

$$R = 2, 10 \tag{66}$$

The results are graphically represented in **Figure 6** to **Figure 9**. Note that for each one of those figures the value of Λ and R are fixed, while Ω and Φ vary for their respective whole assigned range of discrete values specified in equations (63),(64). However, the axis that have been chosen for the representation in the graphs are μ and $\hat{\xi}$ (see equation (54)) instead of Λ and R in order to try to provide a "physical" idea of the final aspect of the loop once the steady state is reached. It must be also commented that for some particular values of the input parameters, no steady state (51) was reached within the integration limit number of time increments, which should be interpreted as a nonlinear resonance with unbounded response. Those points have been removed from these figures. For each one of the figures, for fixed Λ and R, the surface $\varepsilon(\mu,\hat{\xi})$ is represented as isolines. The graphs in the upper row use μ and $\hat{\xi}$ as axis (left) or the 3D view with μ, $\hat{\xi}$ and ε as axis (right). The graphs in the lower row are projections of the same isolines, with the same scale of colours, on the $\hat{\xi}$ and ε axis (left) and on the μ and ε axis (right).

From these figures, for the values of the parameters that have been analysed, some general comments may be made:

-For increasing values of the estimated damping $\hat{\xi}$ (as seen from 0 to 0.8) and decreasing values of frequency ratio μ (from 1 to 0) the error is large and shows a tendency to increase its variability with an upper limit roughly equal to $\hat{\xi}$ (except for the case $\Lambda = 100 \quad R = 10$, that shows the largest errors).

-For values of the frequency ratio μ larger than 1.0, the error is always between 0 and -0.3, independently of the observed values of estimated damping $\hat{\xi}$.

-Again in that range of the frequency ratio μ larger than 1.0, the error is smaller for $\Lambda = 10$ (between 0 and -0.2) than for $\Lambda = 100$ (between 0 and -0.3).

-Combined larger values of Λ and R (which make the loop more similar to a pure friction), increase the variability and amount of error, apart from making more difficult the convergence as it will be shown in the following lines.

After having done all the commented surfaces, the computations were all repeated for a basic number of steps per period increased from the adopted value (49) to

$$N_{pcyc0} = 500 \tag{67}$$

without significant change in the plotted results, except for the case $\Lambda = 100 \quad R = 10$, as it is shown in **Figure 9**. The differences between **Figure 8** and **Figure 9** are only due to the change in the number of steps, which seems to be significant for certain combinations of μ and $\hat{\xi}$. Consequently, for those areas the results should be considered not reliable since a convergence was not reached.

Figure 6 – Tridimensional representation and bidimensional projections of error isolines. Case $\Lambda = 10 \quad R = 2$.

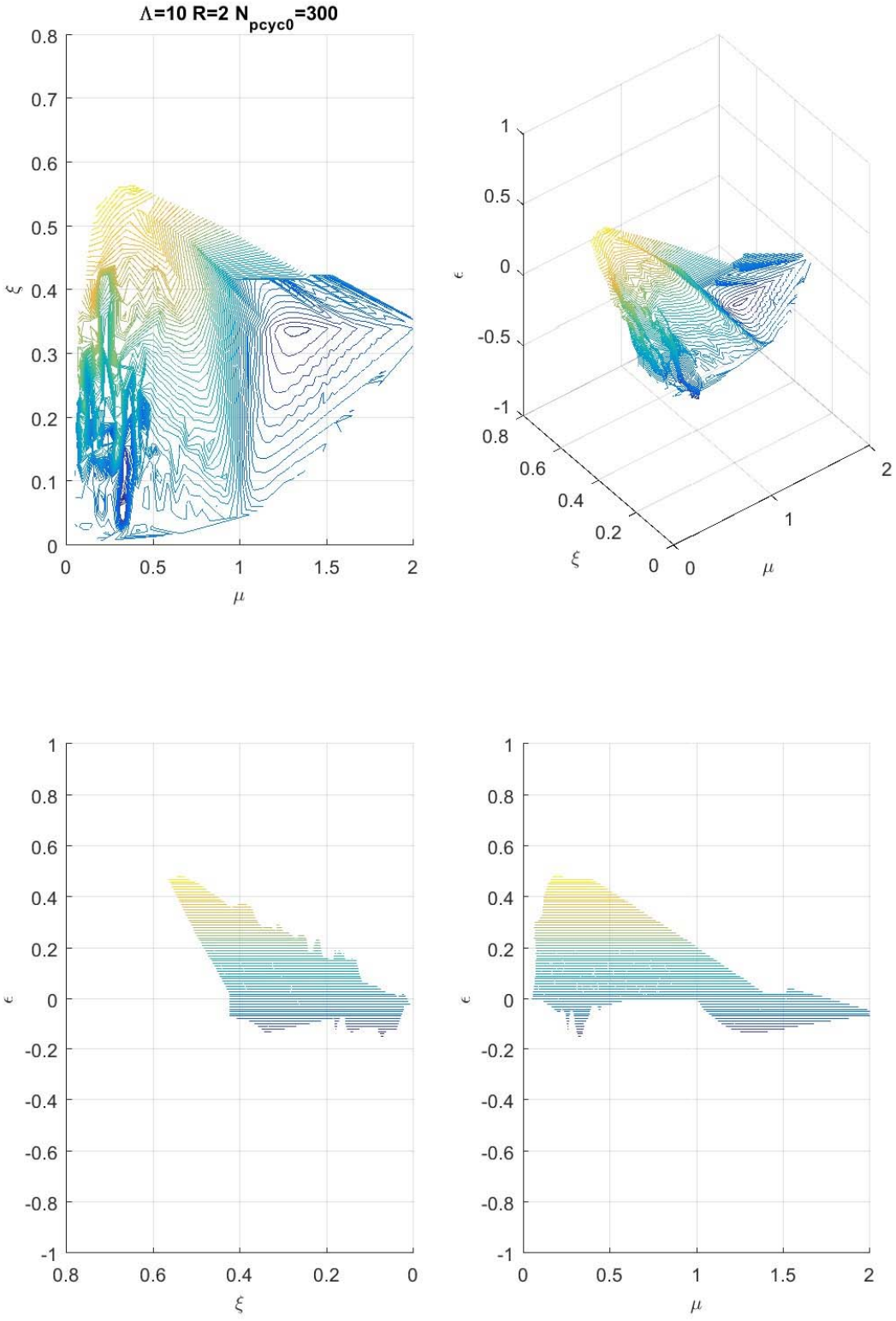

Figure 7 – Tridimensional representation and bidimensional projections of error isolines. Case $\Lambda = 10 \quad R = 10$.

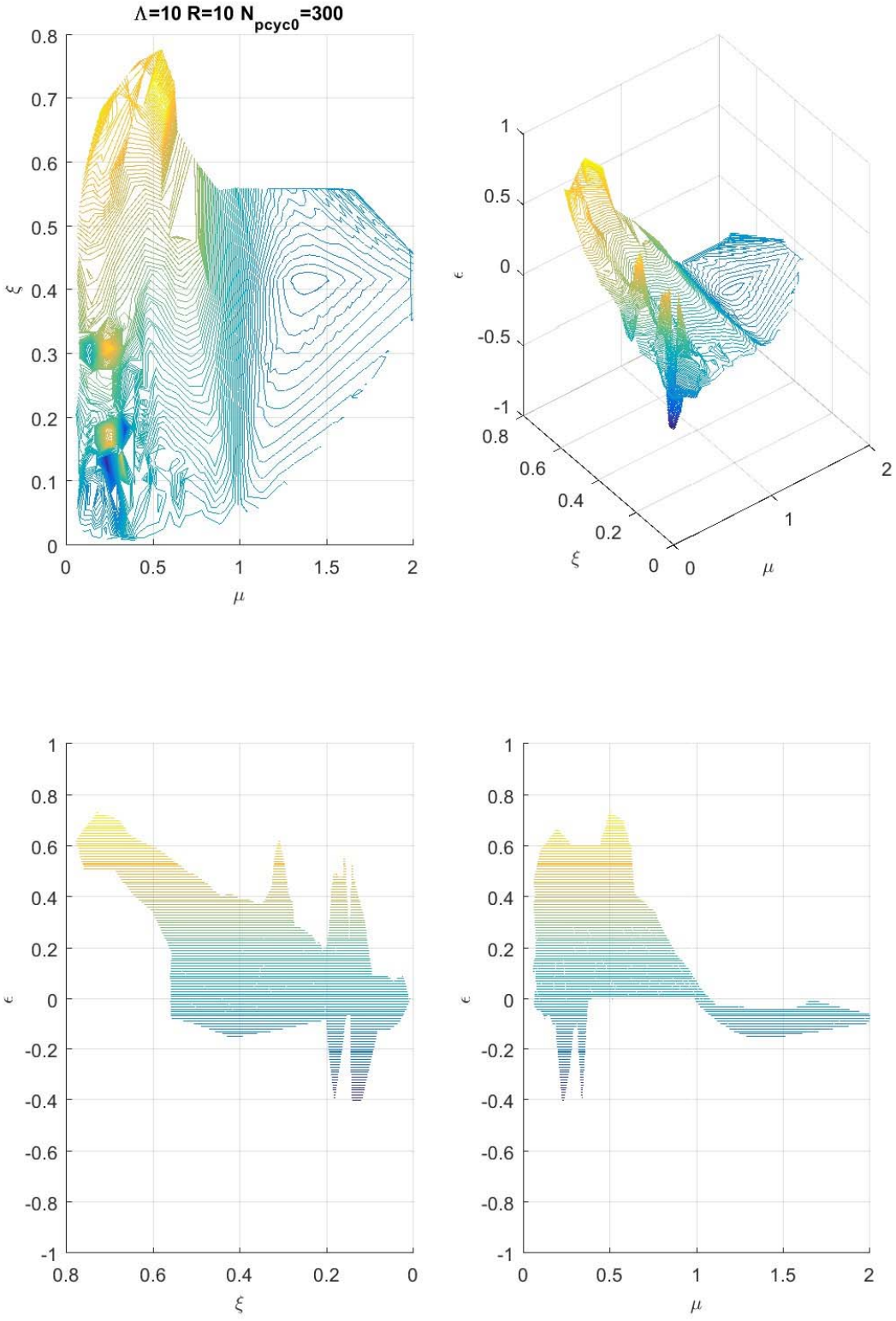

Figure 8 – Tridimensional representation and bidimensional projections of error isolines. Case $\Lambda = 100 \quad R = 2$.

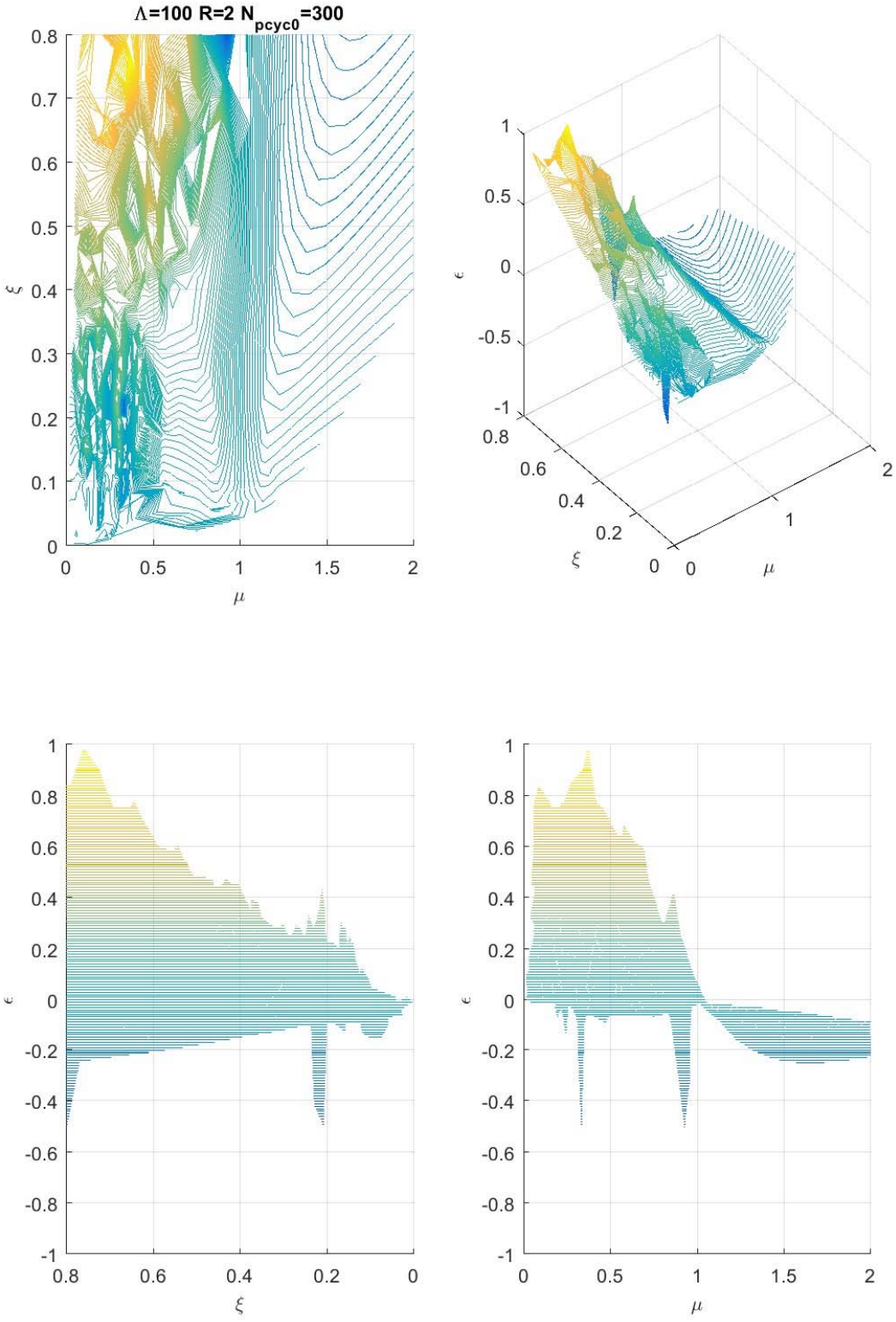

Figure 9 – Tridimensional representation and bidimensional projections of error isolines. Case $\Lambda = 100 \quad R = 10$.

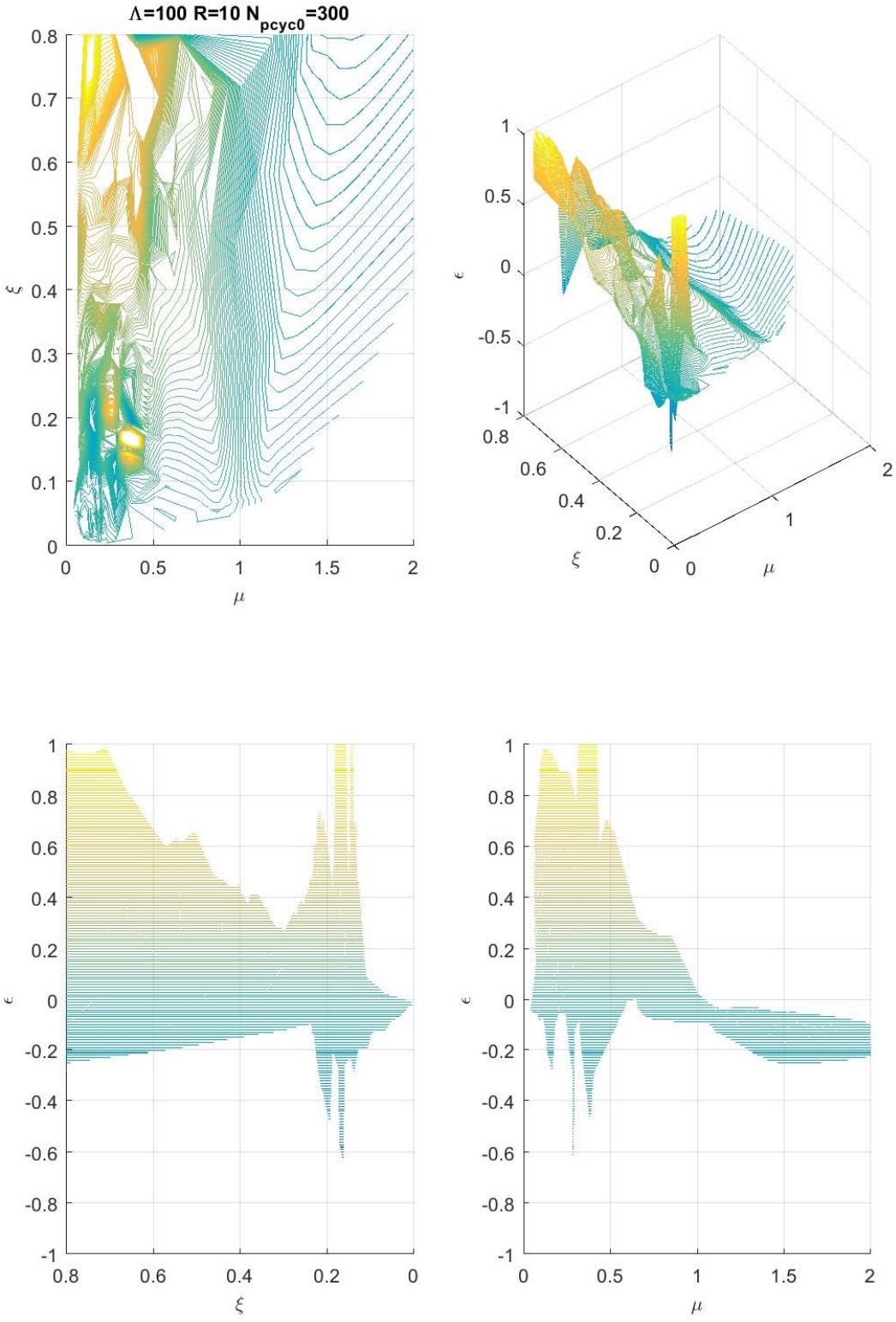

Figure 10 – Repetition of the case in Figure 9 for a larger number of integration steps per period.

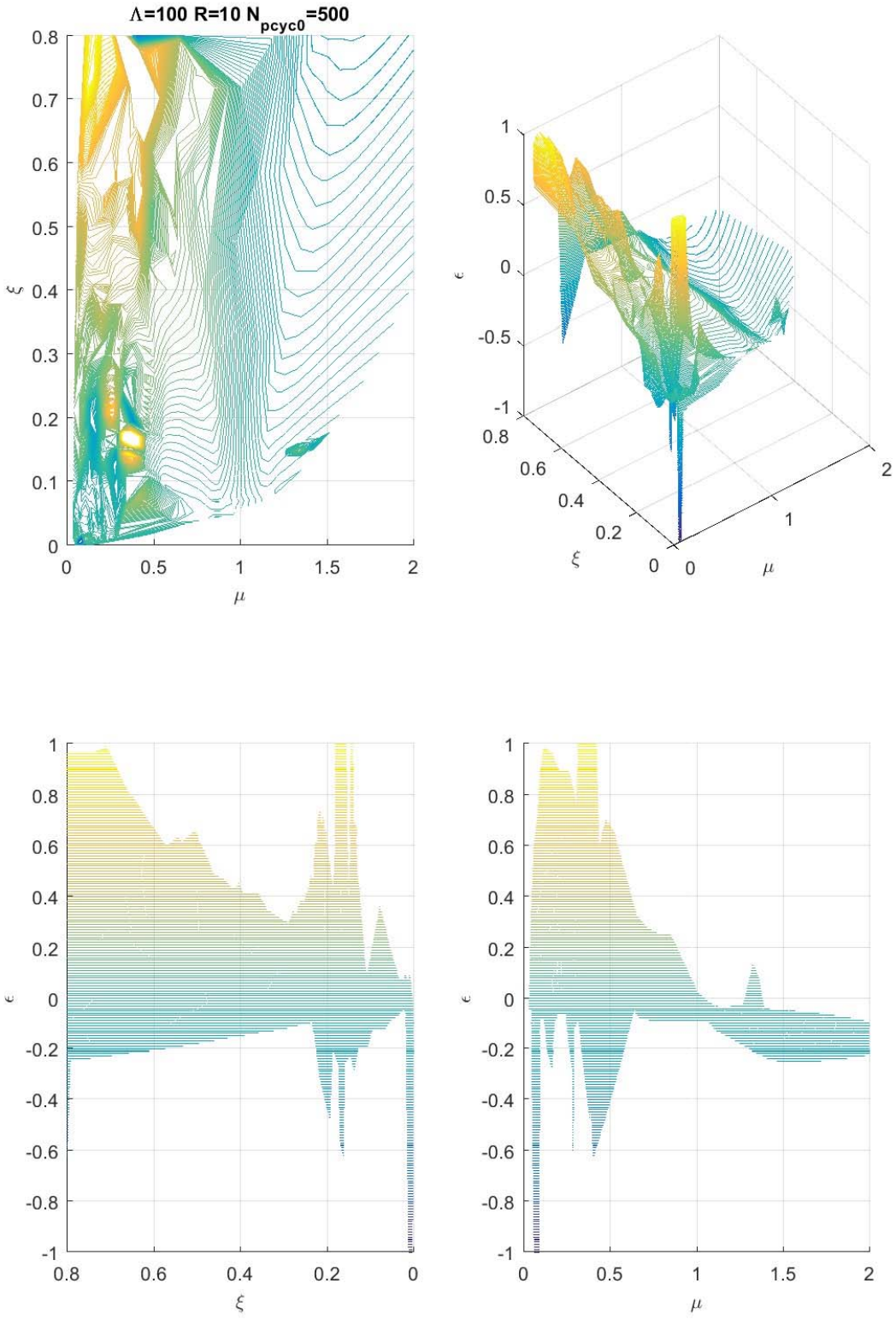

3.4 Some examples

A series of example cases for single value of the parameters $(\Omega, \Phi, \Lambda, R)$ taken from the previous subsection are presented herein.

More precisely, the attention in this subsection is put on the effect of the variation of the parameters

$$\Omega = 0.2, 0.5, 1.0, 2.0 \qquad \Phi = 0.5, 1.0, 2.0 \tag{68}$$

while

$$\Lambda = 10 \qquad R = 2 \tag{69}$$

are kept constant.

From **Figure 11** to **Figure 22**, each figure represents a single case of parameters value as specified in it and contains four graphs of dimensionless variables. The graphs in the upper row are the displacement (left) and force (right) time histories of the last obtained loop from the integration and the ones in the lower row are the restoring force-displacement curve for the whole integration since zero time (left) and just for the last converged cycle (right). Note than in the left graph of the lower row the last cycle is redrawn also on top of the previous ones (red line). At the right graph in the lower row, there is also a dashed straight line that represents the linear regression of the points of that converged loop, being the slope of that line the defined LS effective stiffness computed from the loop points. At the top of that graph, the obtained values of μ, $\hat{\xi}$ and ε are typed.

As commented before, there are cases in which no steady state was reached through the integration and the response continued growing until the limit time period, which should be interpreted as a case of apparent resonance without bounds. One of those cases is represented in **Figure 21**.

As a general comment, we observe from these figures that for this group of cases:

-For constant value of Φ, μ grows with Ω, but $\hat{\xi}$ does not have a monotonous tendency.

-Typically, larger values of $\hat{\xi}$ drive to larger variability of ε, but keeping $|\varepsilon| < \hat{\xi}$.

-The largest errors are observed for combinations of high values of $\hat{\xi}$ and low values of μ as it was seen in the previous section.

-For constant value of Ω, both $\hat{\xi}$ and ε grow almost monotonically with Φ.

Figure 11 –Time histories and restoring force-displacement loops.

Case $\Lambda = 10 \quad R = 2 \quad \Omega = 0.2 \quad \Phi = 0.5$

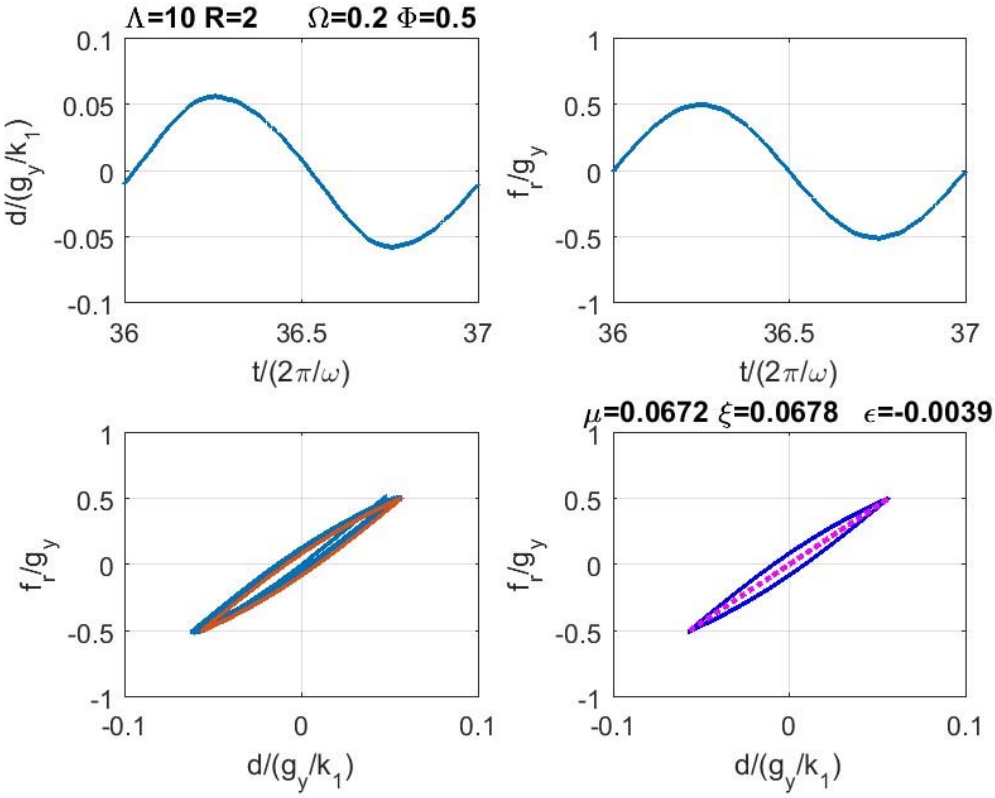

Figure 12 –Time histories and restoring force-displacement loops.

Case $\Lambda = 10 \quad R = 2 \quad \Omega = 0.5 \quad \Phi = 0.5$

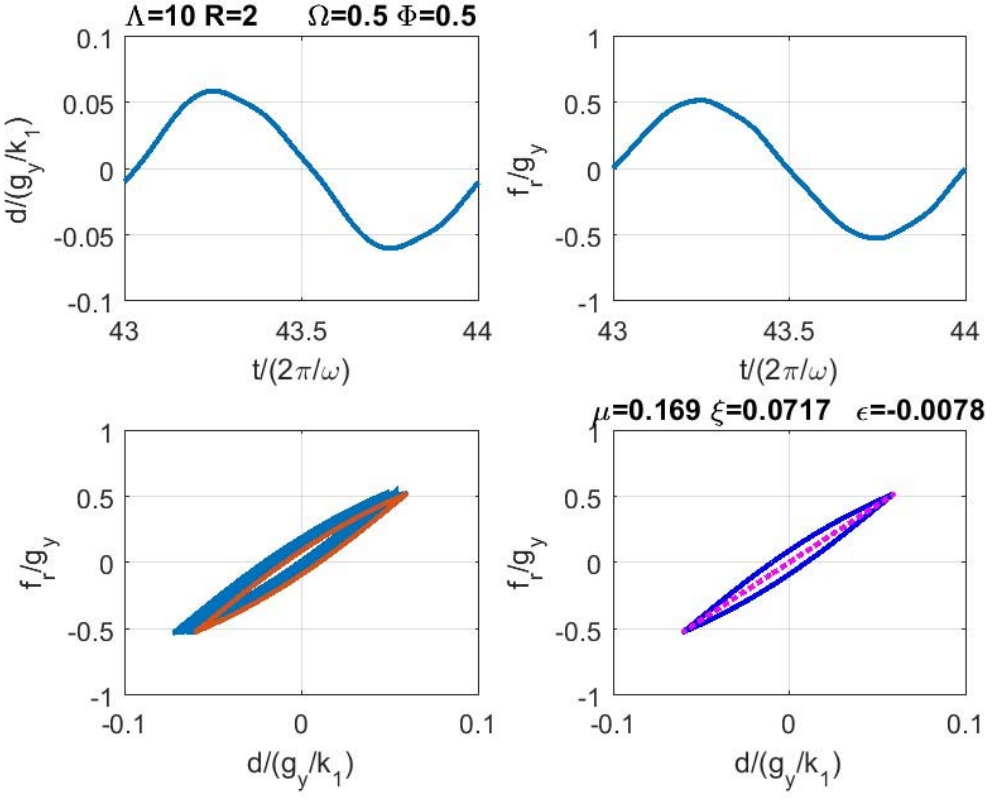

Figure 13 –Time histories and restoring force-displacement loops.

Case $\Lambda = 10 \quad R = 2 \quad \Omega = 1.0 \quad \Phi = 0.5$

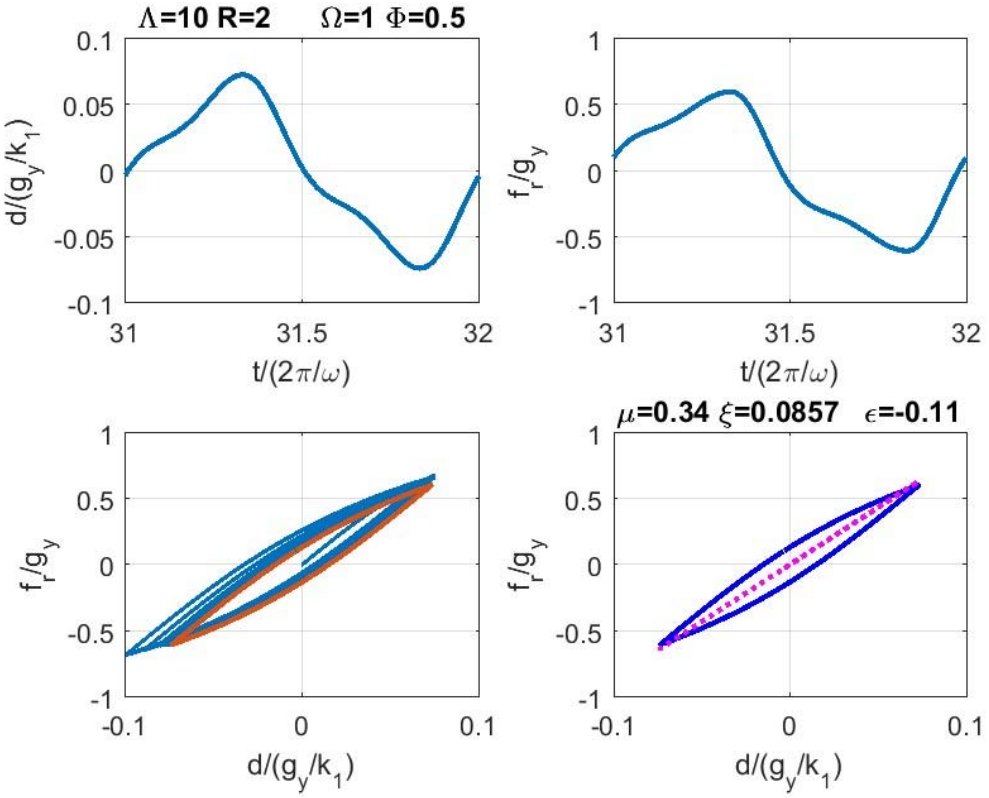

Figure 14 –Time histories and restoring force-displacement loops.

Case $\Lambda = 10 \quad R = 2 \quad \Omega = 2.0 \quad \Phi = 0.5$

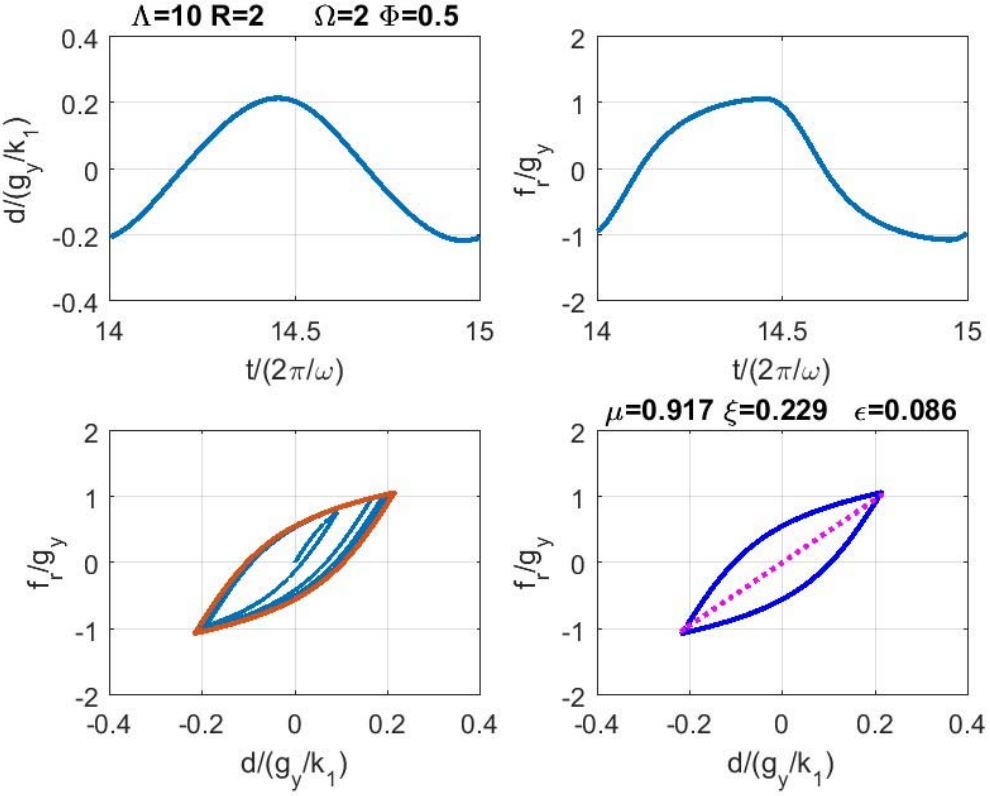

Figure 15 –Time histories and restoring force-displacement loops.

Case $\Lambda = 10 \quad R = 2 \quad \Omega = 0.2 \quad \Phi = 1.0$

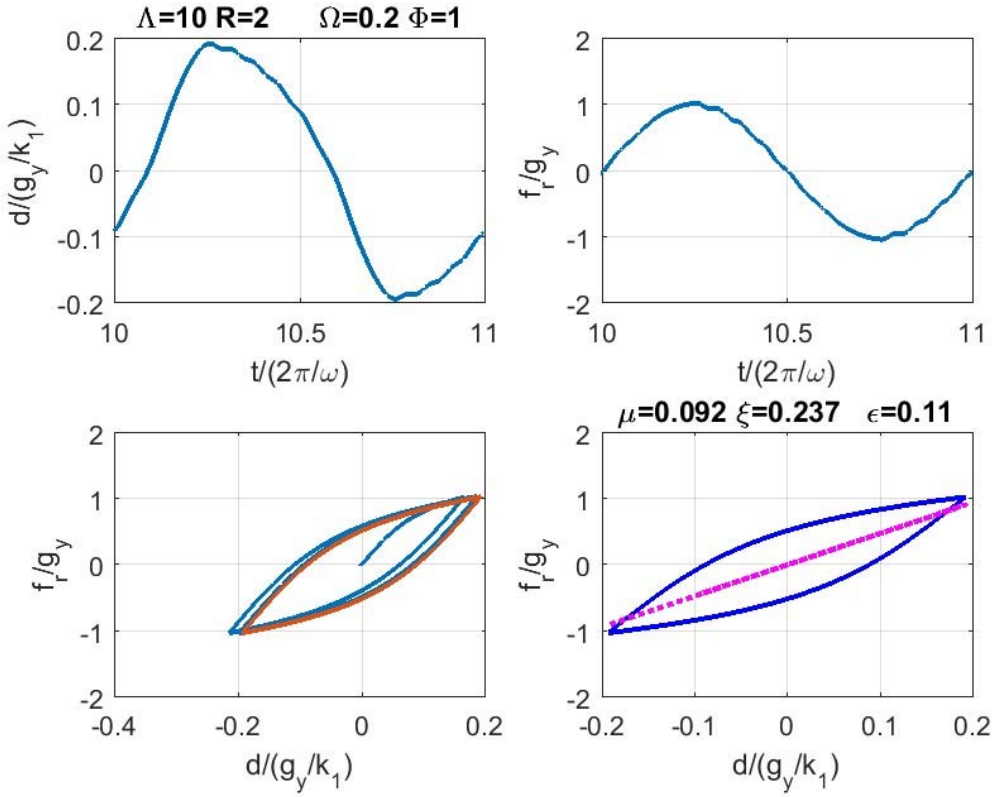

Figure 16 –Time histories and restoring force-displacement loops.

Case $\Lambda = 10 \quad R = 2 \quad \Omega = 0.5 \quad \Phi = 1.0$

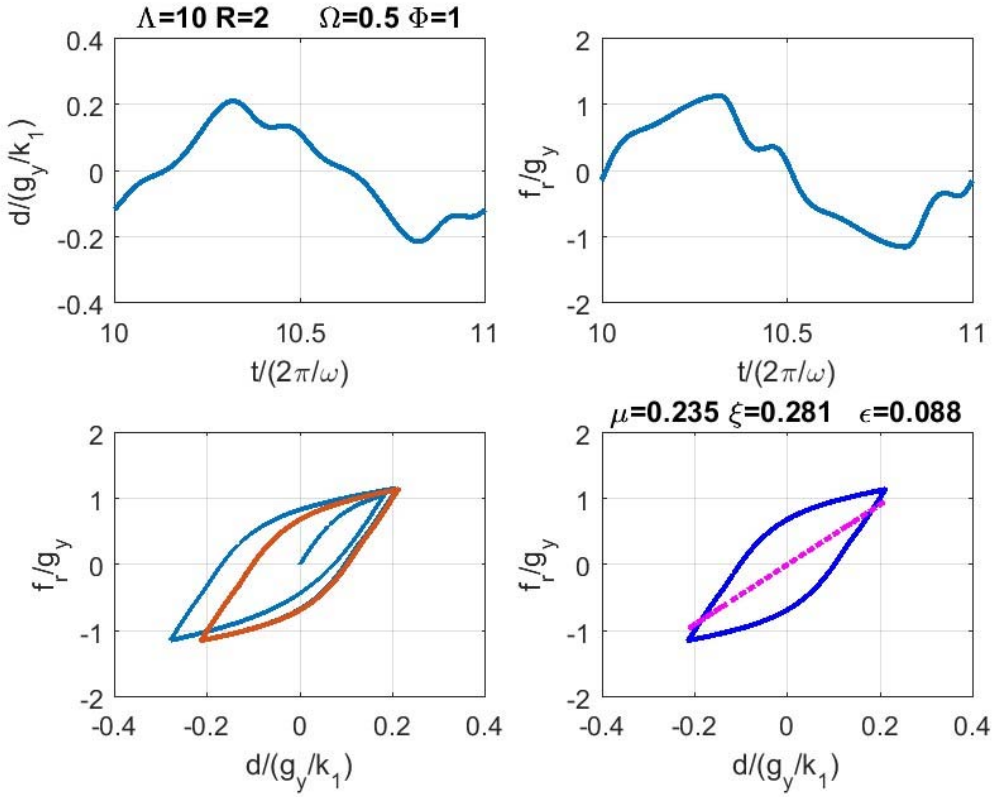

Figure 17 –Time histories and restoring force-displacement loops.

Case $\Lambda = 10 \quad R = 2 \quad \Omega = 1.0 \quad \Phi = 1.0$

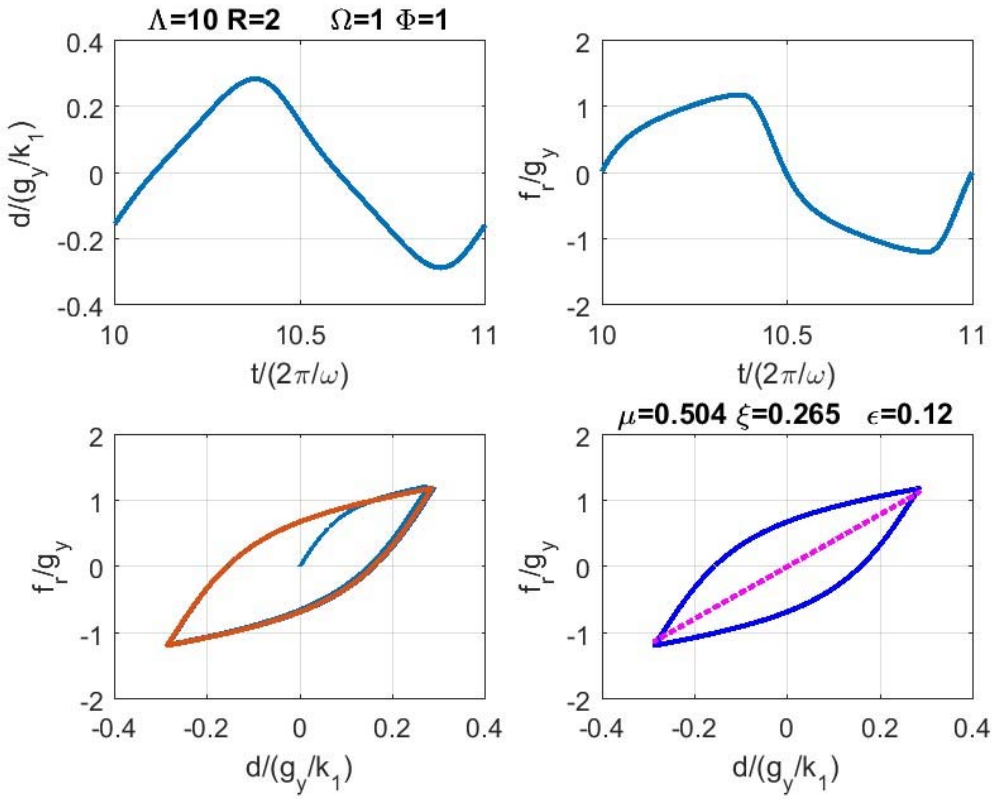

Figure 18 –Time histories and restoring force-displacement loops.

Case $\Lambda = 10 \quad R = 2 \quad \Omega = 2.0 \quad \Phi = 1.0$

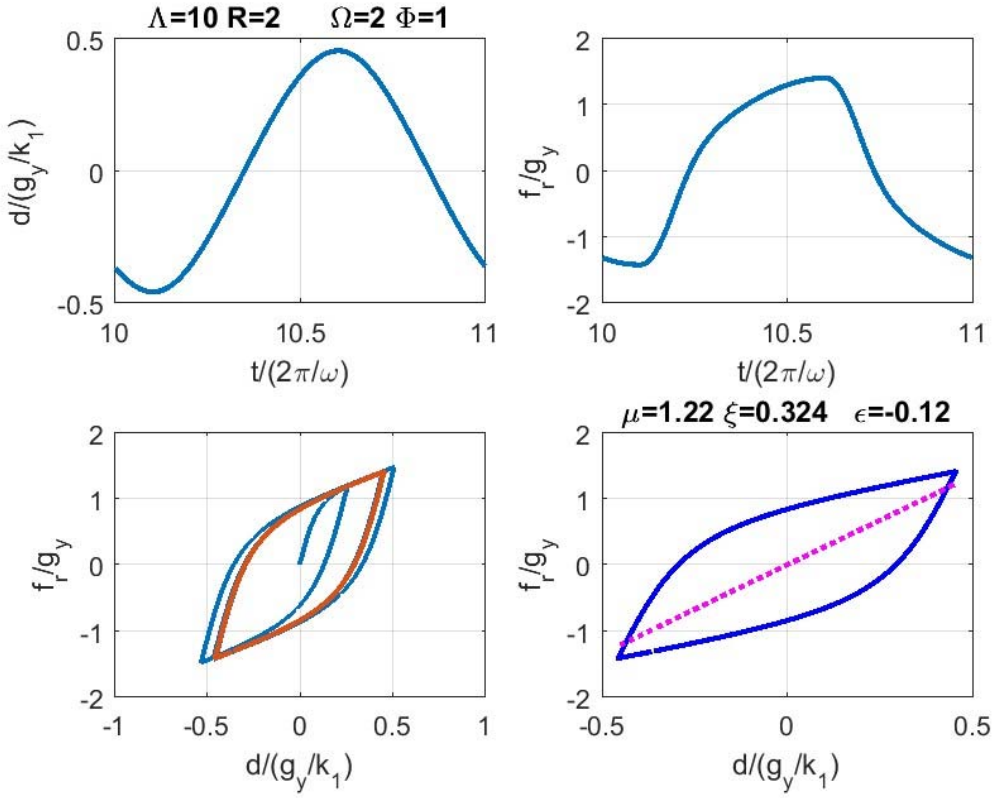

Figure 19 –Time histories and restoring force-displacement loops.

Case $\Lambda = 10 \quad R = 2 \quad \Omega = 0.2 \quad \Phi = 2.0$

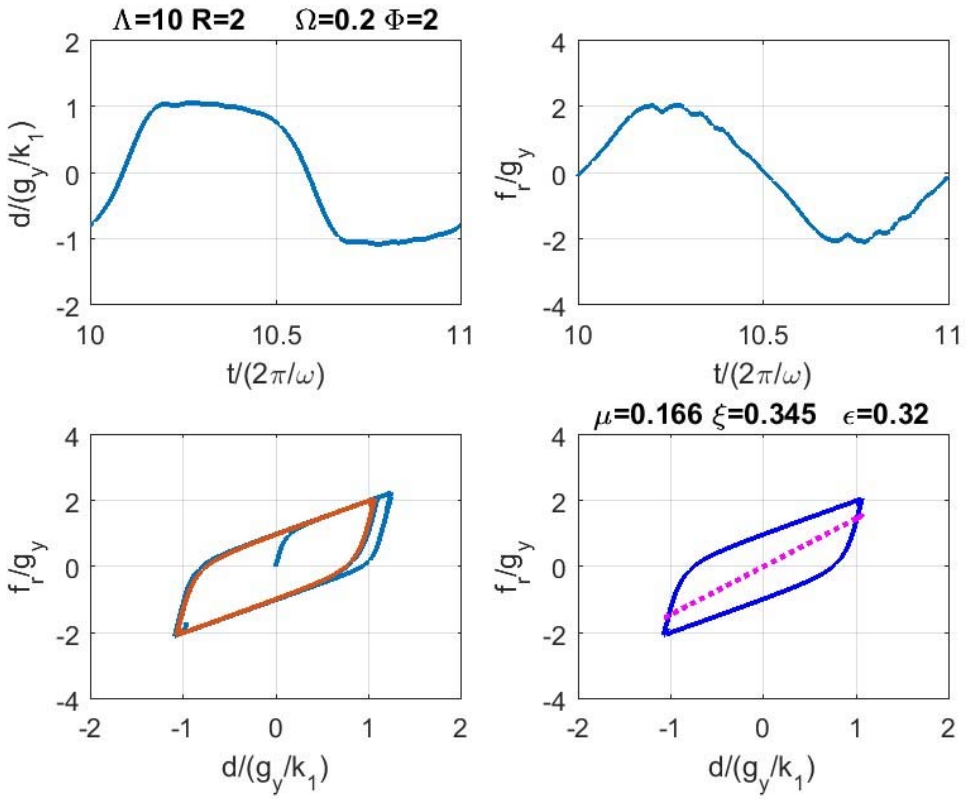

Figure 20 –Time histories and restoring force-displacement loops.

Case $\Lambda = 10 \quad R = 2 \quad \Omega = 0.5 \quad \Phi = 2.0$

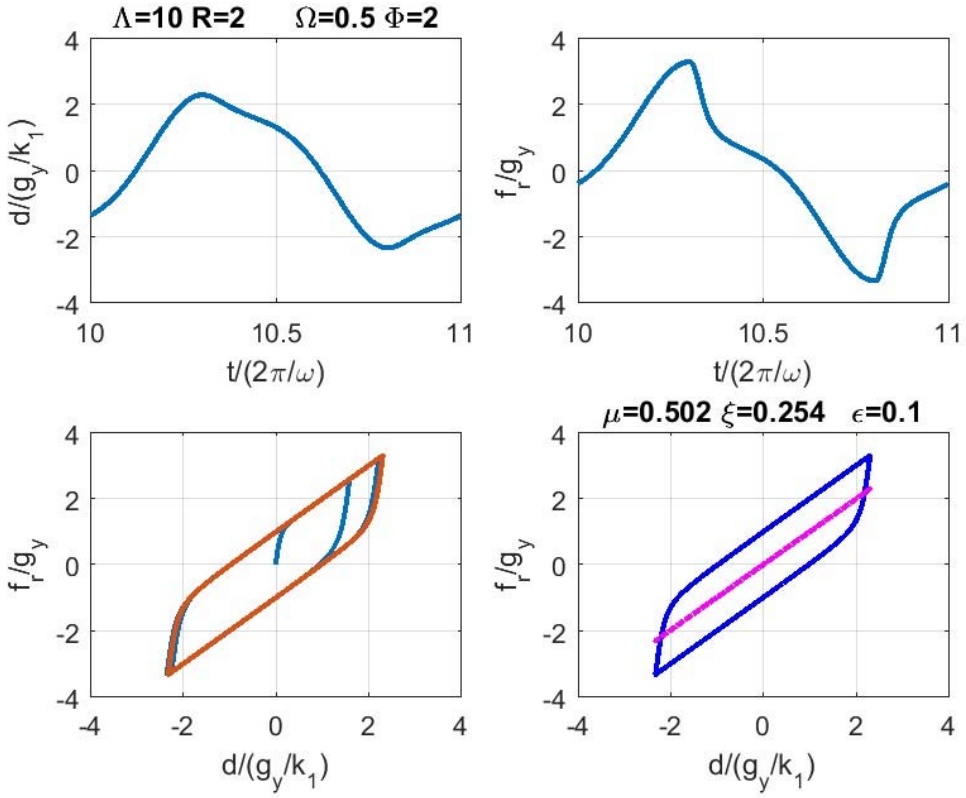

Figure 21 –Time histories and restoring force-displacement loops.

Case $\Lambda = 10 \quad R = 2 \quad \Omega = 1.0 \quad \Phi = 2.0$

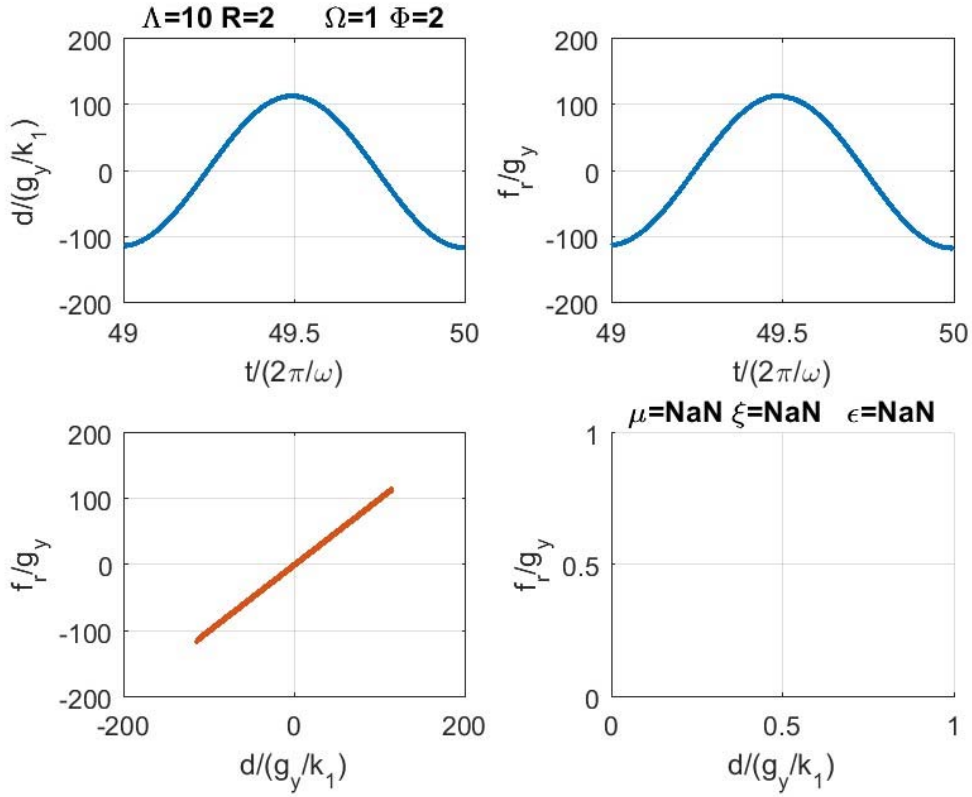

Figure 22 –Time histories and restoring force-displacement loops.

Case $\Lambda = 10 \quad R = 2 \quad \Omega = 2.0 \quad \Phi = 2.0$

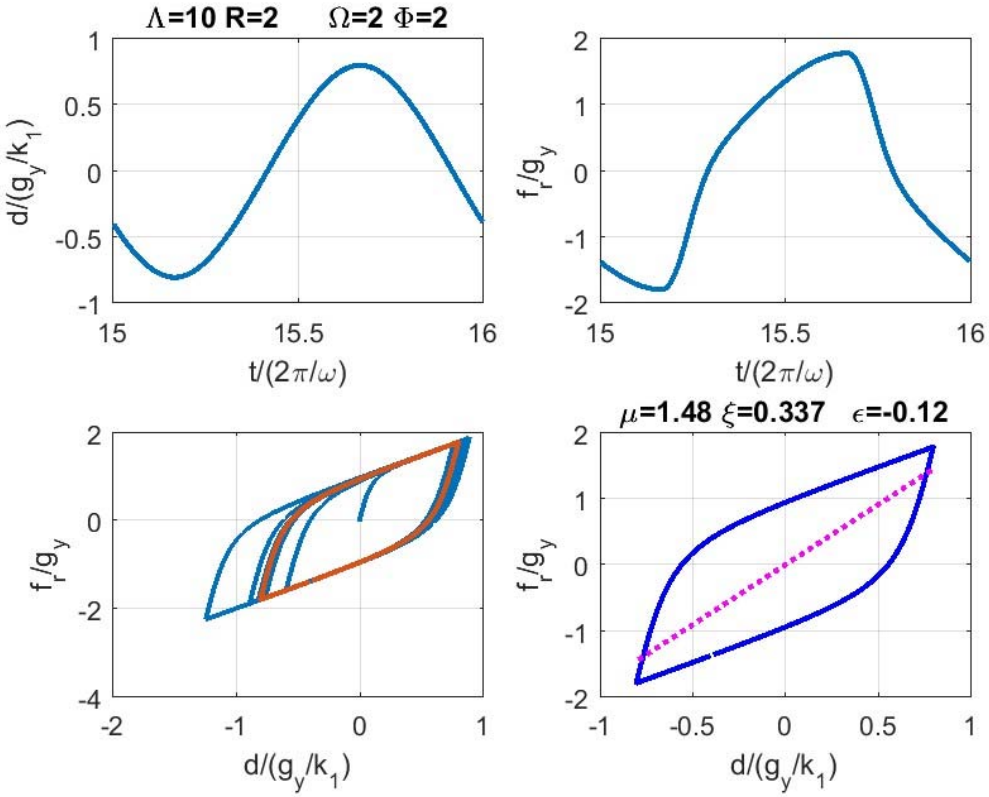

4 CONCLUSIONS

The proposed method for the estimation of equivalent stiffness and damping from a one-degree-of-freedom force-displacement loop is based on a least-square minimization for the computation of the stiffness, which is assumed to be an original approach, while the determination of the damping ratio from the quotient of absorbed to elastic energy is directly taken from the literature.

The reported example error study is based on a particular analytical model and does not use experimental data as it is done in some other studies (Dal Lago and Molina, 2018, for example). The adopted analytical model is based on a Giuffre & Pinto model for the hysteretic part of the force, added to an elastic force following a power law. For the current report the exponent of the power low was kept fixed at 1 (linear elastic force). The most important improvements that could be added to the presented error study are:

- including experimentally obtained force-displacement loops.

- including other models for modelling the hysteresis and not only the Giuffre & Pinto model.

- including transient response and wide-band earthquake-like excitations and not only steady-state response to harmonic load. In fact, these excitations offer more practical interest, but cover a wider generality.

- including other methods for obtaining equivalent stiffness and damping, apart from the one proposed here.

-including other definitions of the error, including predicted forces for example (Dal Lago and Molina, 2018).

References

Dal Lago, B., and Molina, F.J., (2018). Assessment of a capacity spectrum seismic design approach against cyclic and seismic experiments on full-scale precast RC structures, Earthquake Engineering and Structural Dynamics (under review).

Dwairi, H. M. , Kowalsky, M. J. and Nau, J. M.(2007) 'Equivalent Damping in Support of Direct Displacement-Based Design', Journal of Earthquake Engineering, 11: 4, 512-530.

Ewins, D. J. (1984), "Modal Testing: Theory and Practice", RESEARCH STUDIES PRESS LTD., Letchworth, Hertfordshire, England, JOHN WILEY & SONS INC. , New York

Giuffrè A., Pinto P.E. (1970) Il comportamento del cemento armato per sollecitazioni cicliche di forte intensità, Giornale del Genio Civile.

Jacobsen, L. S. (1930) "Steady forced vibrations as influenced by damping," Transactions ASME 52, 169–181.

Menegotto M., Pinto P.E. (1972) Method of analysis for cyclically loaded R.C. frames including changes in geometry and non-elastic behavior of elements under combined normal force and bending, Istituto di Scienza e Tecnica delle Costruzioni, University of Rome, Report 32, October.

Molina, F. J., F. Marazzi, B. Viaccoz, and A. Bosi (2013), "Stability and accuracy in a hybrid test example," Earthquake Engineering and Structural Dynamics, vol. 42, no. 3, pp. 469–475.

Molina, F. J., G. Magonette, P. Pegon, and B. Zapico (2011), "Monitoring damping in pseudo-dynamic tests," Journal of Earthquake Engineering, vol. 15, no. 6, pp. 877–900.

Molina, F. J., P. Pegon, and G. Verzeletti (1999), "Time-domain identification from seismic pseudodynamic test results on civil engineering specimens," in Proceedings of the 2nd International Conference on Identification in Engineering Systems, The Cromwell Press.

Molina, F. J., P. Pegon, and P. Labbé (2016), "Stiffness-Displacement Correlation from the RC Shear Wall Tests of the SAFE Program: Derivation of a Capacity Line Model," Advances in Materials Science and Engineering, vol. 2016, Article ID 5750672, 21 pages, doi:10.1155/2016/5750672

Newmark NM. (1959), A method of computation for structural dynamics. Journal of Engineering Mechanics (ASCE) 67–94.

Priestley M. J. N. (1993) "Myths and fallacies in earthquake engineering – conflicts between design and reality," Bulletin, NZ National Society for Earthquake Engineering 26(3), 329–341.

Rosenblueth E., and Herrera I. (1964) "On a Kind of Hysteretic Damping" ASCE Journal of Engineering Mechanics 90(4), 37–48.

Europe Direct is a service to help you find answers to your questions about the European Union.

Freephone number (*):

00 800 6 7 8 9 10 11

(*) The information given is free, as are most calls (though some operators, phone boxes or hotels may charge you).

More information on the European Union is available on the internet (http://europa.eu).

HOW TO OBTAIN EU PUBLICATIONS

Free publications:

- one copy:
  via EU Bookshop (http://bookshop.europa.eu);
- more than one copy or posters/maps:
  from the European Union's representations (http://ec.europa.eu/represent_en.htm);
  from the delegations in non-EU countries (http://eeas.europa.eu/delegations/index_en.htm);
  by contacting the Europe Direct service (http://europa.eu/europedirect/index_en.htm) or
  calling 00 800 6 7 8 9 10 11 (freephone number from anywhere in the EU) (*).

  (*) The information given is free, as are most calls (though some operators, phone boxes or hotels may charge you).

Priced publications:

- via EU Bookshop (http://bookshop.europa.eu).

KJ-NA-28818-EN-N

JRC Mission

As the science and knowledge service of the European Commission, the Joint Research Centre's mission is to support EU policies with independent evidence throughout the whole policy cycle.

EU Science Hub
ec.europa.eu/jrc

@EU_ScienceHub

EU Science Hub - Joint Research Centre

Joint Research Centre

EU Science Hub

Publications Office

doi:10.2760/40703

ISBN 978-92-79-74073-2